Metal vapour behaviour in thermal plasma of gas tungsten arcs during welding

K. Yamamoto*, M. Tanaka, S. Tashiro, K. Nakata, K. Yamazaki, E. Yamamoto, K. Suzuki and A. B. Murphy

A gas tungsten arc in helium and argon was modelled taking into account the contamination of the plasma by metal vapour from the weld pool. The whole region of gas tungsten arc atmosphere including the tungsten cathode, arc plasma and weld pool was treated using a unified numerical model. A viscosity approximation was used to express the diffusion coefficient in terms of viscosity of shielding gas and metal vapour. The transient two-dimensional distributions of the temperature, velocity of plasma flow and iron vapour concentration were predicted, together with the weld penetration as a function of time for a 150 A arc current at the atmospheric pressure, both for helium and argon welding gases.

It was shown that the thermal plasma in gas tungsten arcs is influenced by iron vapour from the weld pool surface and that the concentration of iron vapour in plasma is dependent on the temperature of the weld pool.

Keywords: Arc, Welding, Steel, Metal vapour, Weld pool, Numerical simulation

Introduction

During arc welding, four states of matter including solid, liquid, gas and plasma, simultaneously exist and mutually interact within a volume of only 1000 mm^3. The temperature widely ranges approximately between 20 000 K in the arc plasma, 3000 K in the tungsten cathode, 2000 K in the molten steel and the room temperature in the surroundings.[1] Owing to a recent remarkable progress in computer simulations and observation techniques, it has become possible to understand the phenomena in arc welding processes quantitatively.[2,3] For example, the authors have developed numerical simulations that calculate the properties of the tungsten cathode, the arc plasma and the weld pool. These simulations have enabled to visually observe a relationship between the formation of a weld pool and the balance of energy and momentum in each state of matter.[4] However, it has not been possible yet to accurately predict the welding parameters, such as the arc voltage and the weld geometry. For a full understanding and precise prediction of these parameters, it is necessary to understand the behaviour of metal vapour in the arc plasma. Figure 1 shows the appearance of helium arcs between a solid tungsten electrode and a solid water cooled copper plate (Fig. 1*a*) and a molten pool in a steel plate (Fig. 1*b*).[5] The former arc is a pure helium arc discharge and the latter represents an arc welding process with helium gas. It is obvious that the state of plasma is different between two cases even under the use of quite similar arc current. The difference is mainly caused by metal vapour from molten steel electrodes. In gas tungsten arc (GTA) welding, it is empirically known that the amount of smut or soot stuck on weld beads greatly differs in shielding between argon and helium. It is furthermore known that the arc voltage in GTA on water cooled copper differs from that in GTA welding. The cause of these phenomena is the metal vapour from the weld pool.

Metal atoms generally have more states of low energy excitation and more likely to be ionised than atoms of shielding gases such as argon and helium. These characteristics contribute to an increase in the radiative emission coefficient and electric conductivity of plasma. It is estimated that the former affects the thermal pinch effect and electric conductivity of plasma and that the latter affects the current density distribution. Tashiro *et al.*[5] conducted a virtual experiment by numerically simulating a pure helium arc and an arc in helium uniformly mixed with 30 mol.-% iron atoms, and showed that an obvious arc constriction occurred in the latter case. They further reported that the energy efficiency greatly decreased approximately from 80 to 35%. These results suggest that the existence of metal vapour changes the heat source property in arc welding processes and consequently changes the size and the shape of a molten pool.

As noted above, there have been significant advances in the simulation of arc welding.[6–14] Most early numerical models have treated either only the arc plasma[6,7] or only the weld pool[8–13] without metal vapour consideration. Recently, the completely unified model of gas metal arc with the formation of droplets

Joining and Welding Research Institute, Osaka University, 11-1 Mihogaoka Ibaraki, Osaka 567-0047, Japan

*Corresponding author, email k-yama@jwri.osaka-u.ac.jp

Published by Maney on behalf of the Institute
Received 22 January 2008; accepted 19 April 2008
DOI 10.1179/174329308X319235

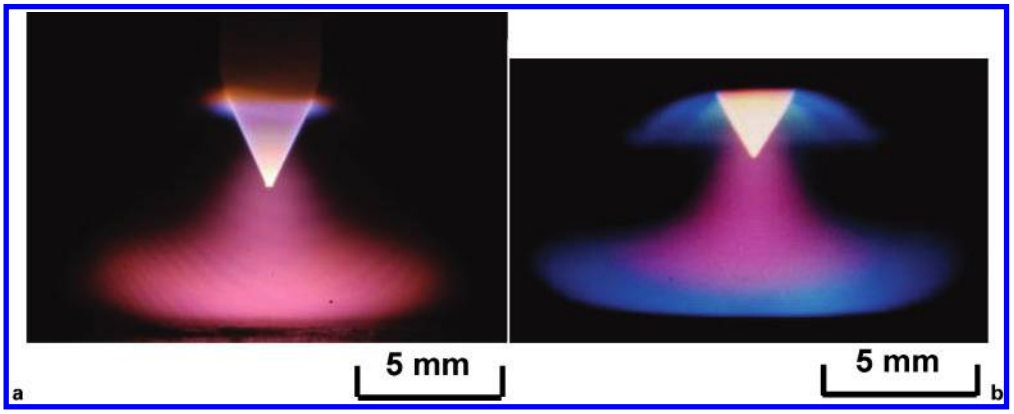

a He TIG with water cooled Cu; *b* He TIG with stainless steel

1 Effect of metal vapour from molten electrodes on helium arc plasma for 150 A

from a steel wire electrode and also the weld pool has been reported.[14] However, this simulation is for the pure argon gas shielding and the effect of metal vapour is not considered. Meanwhile, calculations of the behaviour of metal vapour in atmospheric plasma have also been reported.[15] However, the conditions in these calculations are far from those in actual welding because a solid electrode with the constant temperature is assumed. It is important for accurate understanding of the arc welding process to consider the mixing of the metal vapour in a model that takes into account the tungsten cathode, the arc plasma and the weld pool.

In the present paper, the authors use a numerical model of stationary GTA welding taking into account the iron vapour produced from the weld pool surface, and they simulate transient changes in the distribution of the metal vapour, the plasma temperature and the formation of the weld pool in GTA welding.

Simulation model

This model is concerned with the stationary GTA welding using a tungsten cathode of 3·2 mm diameter with a 60° conical tip. Figure 2 shows the calculation domain described in the two-dimensional cylindrical coordinate assuming rotational symmetry around the arc axis. The anode is the water cooled copper or stainless steel. Stainless steel is extensively welded with the GTA welding process because stainless steel is protected from the atmosphere by the inert gas.[16] Helium or argon shielding gas is supplied from the outside of the cathode on the upper boundary at the flow rate of $5{\cdot}0\times10^5$ mm^3 s^{-1} for helium and $1{\cdot}7\times10^5$ mm^3 s^{-1} for argon.

The time dependant two-dimensional calculations are conducted. The governing equations used in the model are shown as follows.

The mass continuity equation is

$$\frac{\partial\rho}{\partial t}+\frac{1}{r}\frac{\partial}{\partial r}(r\rho v_r)+\frac{\partial}{\partial z}(\rho v_z)=0 \tag{1}$$

The radial momentum conservation equation is

$$\frac{\partial\rho v_r}{\partial t}+\frac{1}{r}\frac{\partial}{\partial r}(r\rho v_r^2)+\frac{\partial}{\partial z}(\rho v_z v_r)=-\frac{\partial p}{\partial r}-j_z B_\theta+\frac{1}{r}\frac{\partial}{\partial r}\left(2r\eta\frac{\partial v_r}{\partial r}\right)+\frac{\partial}{\partial z}\left(\eta\frac{\partial v_r}{\partial z}+\eta\frac{\partial v_z}{\partial r}\right)-2\eta\frac{v_r}{r^2} \tag{2}$$

The axial momentum conservation equation is

$$\frac{\partial\rho v_z}{\partial t}+\frac{1}{r}\frac{\partial}{\partial r}(r\rho v_r v_z)+\frac{\partial}{\partial z}(\rho v_z^2)=-\frac{\partial p}{\partial z}-j_r B_\theta+\frac{\partial}{\partial z}\left(2\eta\frac{\partial v_z}{\partial r}\right)+\frac{1}{r}\frac{\partial}{\partial r}\left(r\eta\frac{\partial v_r}{\partial z}+r\eta\frac{\partial v_z}{\partial r}\right)+\rho g \tag{3}$$

The energy conservation equation is

$$\frac{\partial\rho h}{\partial t}+\frac{1}{r}\frac{\partial}{\partial r}(r\rho v_r h)+\frac{\partial}{\partial z}(\rho v_z h)=\frac{1}{r}\frac{\partial}{\partial r}\left(\frac{r\kappa}{c_p}\frac{\partial h}{\partial r}\right)+\frac{\partial}{\partial z}\left(\frac{\kappa}{c_p}\frac{\partial h}{\partial r}\right)+j_r E_r+j_z E_z-U \tag{4}$$

The current continuity equation is

$$\frac{1}{r}\frac{\partial}{\partial r}(rj_r)+\frac{\partial}{\partial z}(j_z)=0 \tag{5}$$

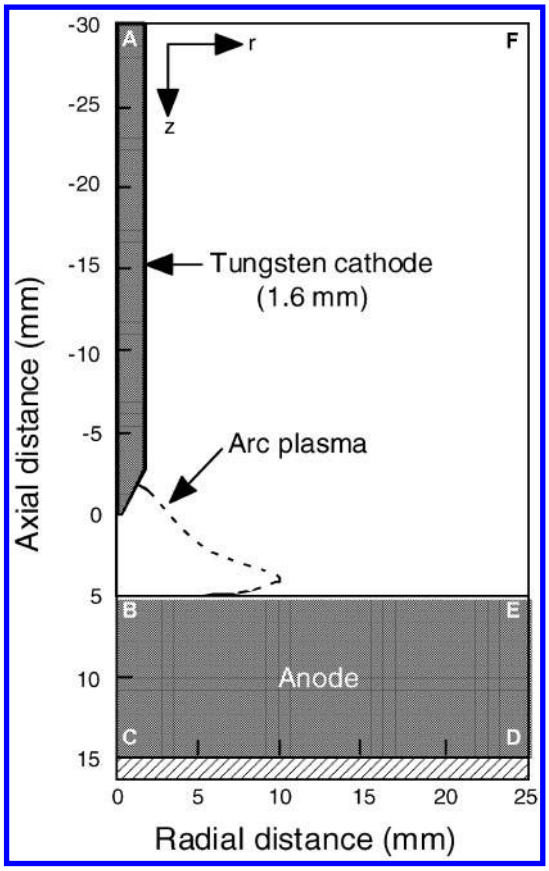

2 Schematic illustration of simulation domain

$$j_r = -\sigma E_r, j_z = -\sigma E_z \tag{6}$$

where t is time, h is enthalpy, p is pressure, v_r and v_z are radial and axial velocities, j_r and j_z are the radial and axial components of the current density, g is acceleration due to gravity, c_p is specific heat, κ is thermal conductivity, ρ is density, η is viscosity, U is radiative emission coefficient and σ is electrical conductivity. E_r and E_z are the radial and axial components of the electric field defined by

$$E_r = -\frac{\partial V}{\partial r}, E_z = -\frac{\partial V}{\partial z} \tag{7}$$

where V is electric potential.

The azimuthal magnetic field B_θ induced by arc current is evaluated by Maxwell's equation

$$\frac{1}{r}\frac{\partial}{\partial r}(rB_\theta) = \mu_0 j_z \tag{8}$$

where μ_0 is the permeability of free space.

It is necessary to consider the effects of energy transfer at the electrode surfaces. The additional energy fluxes at the cathode and anode are described as

$$\text{Cathode}: F_K = -\varepsilon\alpha T^4 - |j_e|\phi_K + |j_i|V_i \tag{9}$$

$$\text{Anode}: F_A = -\varepsilon\alpha T^4 - |j|\phi_A \tag{10}$$

where ε is surface emissivity, α is the Stefan–Boltzmann constant, ϕ_K is the work function of the tungsten cathode, V_i is the ionisation potential of the plasma gas, j_e is the electron current density, j_i is the ion current density, ϕ_A is the work function of the anode and T is the temperature. For the cathode surface, F_K needs to be included in equation (4) to take into account the thermionic cooling by emission of electrons, radiative cooling and ion heating. Similarly, for the anode surface, F_A is required in equation (4) to take into account radiative cooling and thermionic heating. Furthermore, for the cathode surface, the electron current and the ion current are considered separately and defined based on the Richardson–Dushman equation of thermionic emission as follows

$$j_R = AT^2 \exp\left(-\frac{e\phi_K}{k_B T}\right) \tag{11}$$

where k_B is the Boltzmann's constant and A is the Richardson's constant, which depend on the cathode material. The ion current density j_i is then assumed to be $j_i = j - j_R$, where the total current density j is $|j| = |j_e| + |j_i|$.

The convection in the weld pool is influenced by the shear stress caused by the convective flow of the cathode jet, the Marangoni force induced by the gradient in the surface tension of the weld pool, the buoyancy due to gravity and the electromagnetic pinch force due to the arc current. If only the driving forces of the weld pool convection at the boundary between the weld pool and the arc plasma are considered, the shear stress caused by the plasma flow is already included in η in equation (2). Therefore, only the Marangoni force is added, which is given by[4]

$$M_A = \frac{\partial}{\partial z}\left(\frac{\partial \gamma}{\partial T}\frac{\partial T}{\partial r}\right) \tag{12}$$

where γ is the surface tension of the weld pool. It is assumed in this study that the stainless steel contains sulphur as low as 10 ppm and that the variation of the surface tension at the weld pool surface decreases linearly with increasing temperature ($\partial\gamma/\partial T = -0{\cdot}46$ mN/mK).[4]

A mass conservation equation expressed by equation (13) is applied to take a metal vapour behaviour into account.[7] In practice, Fe, Cr, Ni and Mn[17] are included as metal vapour in an arc plasma because stainless steel is used. However, only iron vapour is taken into account in this study to simplify the model and facilitate calculation

$$\frac{\partial}{\partial t}(\rho C_1) + \frac{1}{r}\frac{\partial}{\partial r}(r\rho v_r C_1) + \frac{\partial}{\partial z}(\rho v_z C_1) = \frac{1}{r}\frac{\partial}{\partial r}\left(r\rho D\frac{\partial C_1}{\partial r}\right) + \frac{\partial}{\partial z}\left(\rho D\frac{\partial C_1}{\partial z}\right) \tag{13}$$

where C_1 is mass fraction concentration of iron vapour and D is the two-dimensional diffusion coefficient which is expressed by the viscosity approximation equation

$$D = \frac{2(2)^{1/2}(1/M_1 + 1/M_2)^{0{\cdot}5}}{\left[\left(\rho_1^2/\beta_1^2\eta_1^2 M_1\right)^{0{\cdot}25} + \left(\rho_2^2/\beta_2^2\eta_2^2 M_2\right)^{0{\cdot}25}\right]^2} \tag{14}$$

where M_1 and M_2 are the molecular weights of iron and the shielding gas respectively. ρ_1, ρ_2, η_1 and η_2 are the density and viscosity of iron and the shielding gas respectively. β_1 and β_2 are the dimensionless constants defined as $\beta_i = (D_{ii}\rho_i)/\eta_i$, and theoretically range between 1·2 to 1·543 for various kinds of gas such as Ar, He, H_2, N_2, O_2 and CO_2. $\beta_1 = \beta_2 = 1{\cdot}385$ is assumed based on the mean value of the experimental data.[18] The viscosity approximation is relatively accurate up to 30 000 K[19] because viscosity which is calculated as a plasma property takes ionised matters into account, and then it is considered to be suitable for modelling welding arcs.

C_1 is set to be zero in the cathode area and in the solid area of the anode. However, at the anode surface where the temperature is above the melting point, C_1 is given as[15]

$$C_1 = \frac{p_{v,1}M_1}{p_{v,1}M_1 + (p_{atm} - p_{v,1})M_2} \tag{15}$$

where p_{atm} is the atmospheric pressure, and $p_{v,1}$ is the iron vapour partial pressure which is a function of the weld pool temperature.[20] According to equation (15), C_1 varies between zero and 1·0. For the other boundary conditions, $C_1 = 0$ at lines AF and FE shown in Fig. 2, and $(\partial C_1/\partial r) = 0$ at the arc axis (AB).

In the present model, plasma properties are dependent on not only the temperature but also the mole fraction of iron vapour. The plasma properties at the intermediate concentrations of iron vapour are calculated using a linear approximation based on the properties at 0, 1, 10, 20 and 30 mol.-% of iron vapour mixture rate.[12] The properties were calculated using the Chapman–Enskog approximation[21] under the assumption that the arc plasma is in a local thermodynamic equilibrium (LTE) condition. All of electron temperature, ion temperature and heavy particle temperature are the same in the LTE condition. For example, the electrical conductivities and the radiative emission coefficients, which are significantly affected by the mixture of iron vapour, are shown in Figs. 3 and 4 respectively. As

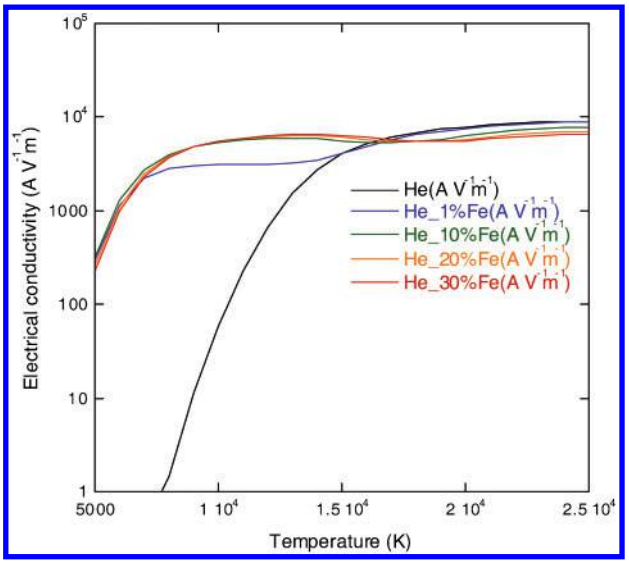

3 Dependence of electrical conductivities of helium gas on temperature for each mixing ratio

shown in Fig. 3 concerning the change in electrical conductivity of helium plasma, electrical conductivity greatly increases by the addition of iron vapour at the temperatures below 15 000 K and the effect of the iron vapour addition does not differ between 1, 10, 20 and 30% of the mixing ratio. Figure 4 shows the change in the radiative emission coefficient. The radiative emission coefficient increases with increased mixing ratio of iron vapour while it remains in a very low level for pure helium plasma.

The governing and auxiliary equations were solved iteratively by the SIMPLEC numerical procedure. The other approximations and boundary conditions are given in present authors' previous papers.[5,22]

Results

The present model was applied to the case of stationary helium GTA welding of stainless steel. Figure 5 shows the two-dimensional distribution of the temperature, weld penetration, fluid flow velocity and mole fraction of iron vapour at 20 s after arc ignition, namely when

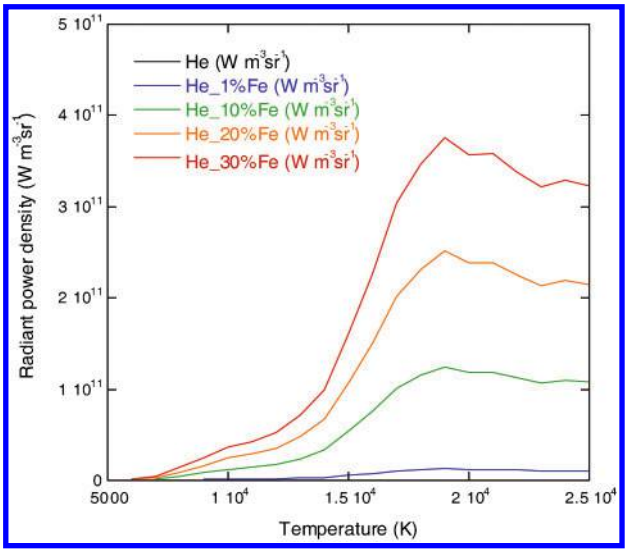

4 Dependence of radiant power density of helium gas on temperature for each mixing ratio

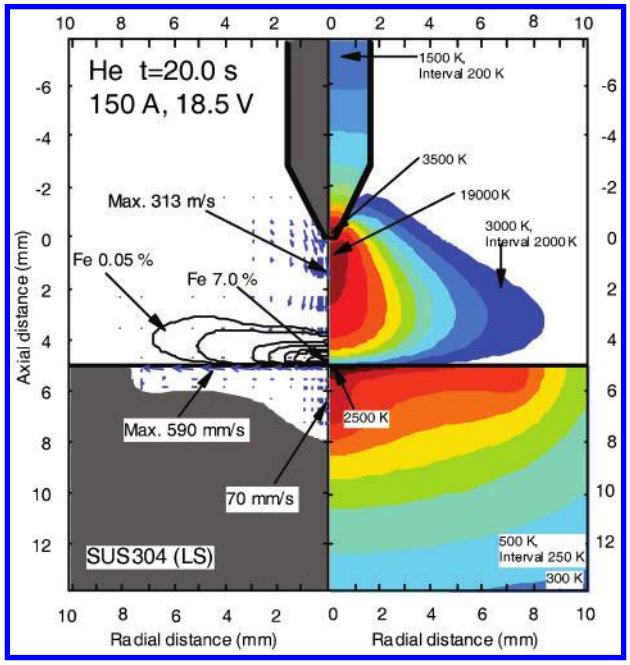

5 Calculated results for helium GTA welding for 150 A at 20 s after arc ignition

the weld pool has grown to a sufficient extent although the weld pool does not reach steady state.[23] The distribution of iron vapour is determined by the diffusion term and the convection term as described in equation (13). In an arc atmosphere where high speed plasma flow of 300 m s^{-1} exists, the convection term dominates. It is thus seen that distribution of iron vapour expands in the radial direction, concentrating just above the weld pool surface. The concentration of iron vapour mixed in arc plasma attains to 7 mol.-%. This result is in good agreement with the experimental data by Terasaki.[17]

Figure 6 shows calculated and experimental arc voltage for water cooled copper and stainless steel anodes at 20 s after arc ignition when arc current was varied at 50, 100, 150 and 200 A. The calculations appear to be consistent with the experiments. The work

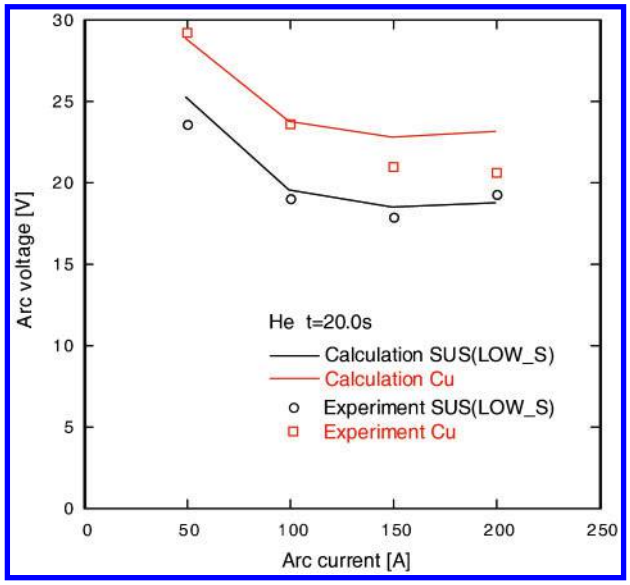

6 Comparison of calculated arc voltage with experimental results

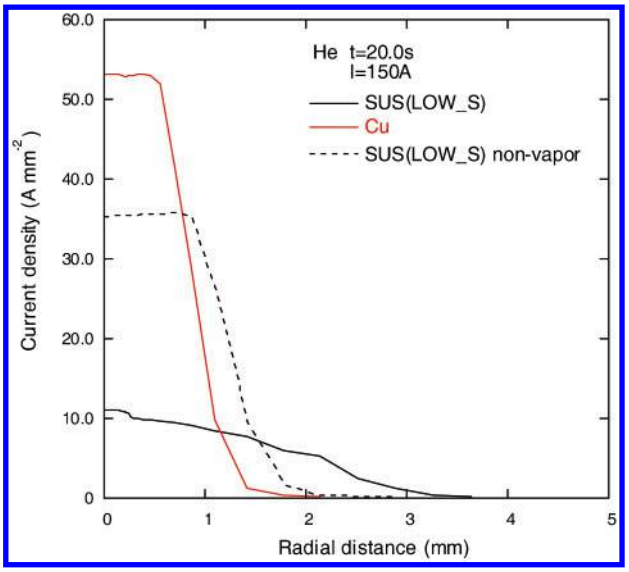

7 Comparison of calculated current densities at anode surface

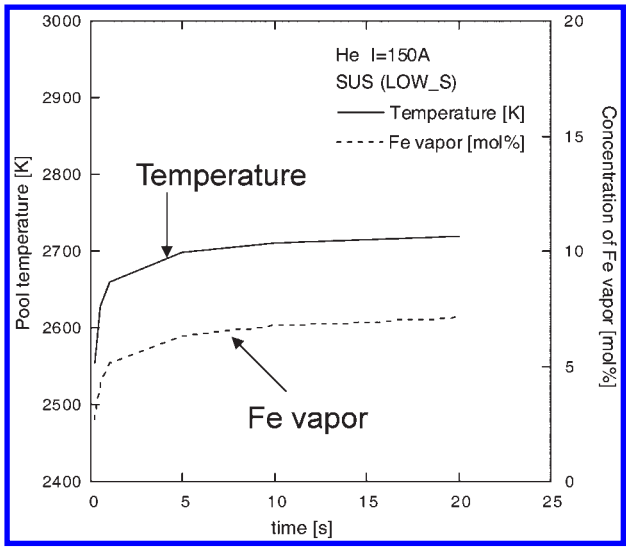

9 Relation between maximum weld pool temperature and maximum concentration of iron vapour in helium GTA welding

piece was a SUS304 stainless steel plate of 50 mm in width, 100 mm in length and 10 mm in thickness on a water cooled copper plate. The steel contains sulphur of 10 ppm. The welding conditions of the arc length, electrode diameter and flow rate of shielding gas were the same as those in the calculation. Figure 6 shows that the arc voltage for the stainless steel anode is $\sim$5 V lower than that for the water cooled copper anode in the whole arc current range. This is due to the effect of iron vapour from the weld pool. As shown in Fig. 3, a very small amount of iron vapour increases the electrical conductivity. As a result, the voltage gradient decreases and the arc voltage lowers particularly just above the weld pool. It is known that GTA welding with helium gas shows negative load resistance characteristics in the low current range. Both calculated and experimental results demonstrate this tendency. A small difference from 2 to 3 V appeared in the current range of 100 to 200 A between the calculation and experiment in the case of the water cooled copper anode. A likely reason for this difference is that a small amount of cupper vapour is produced from the anode surface at high current range where heat input density is raised and resultantly decreases arc voltage in the experiments.

Figure 7 shows calculated current density distributions at the anode surface for the water cooled copper anode and stainless steel anode. For the stainless steel anode, the distribution calculated neglecting the effect of iron vapour on the arc plasma is also shown to demonstrate the influence of iron vapour. The peak current density exceeds 50 A mm^{-2} in the case of the water cooled copper anode. The calculated current density distribution for the stainless steel anode obviously differs between when the existence of iron vapour is not neglected and when neglected. The peak current density when iron vapour is neglected is over

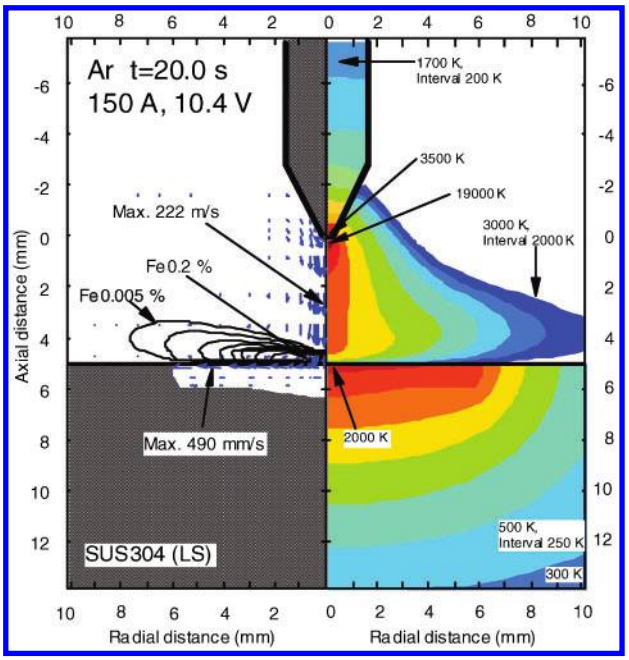

8 Calculated results for argon GTA welding for 150 A at 20 s after arc ignition

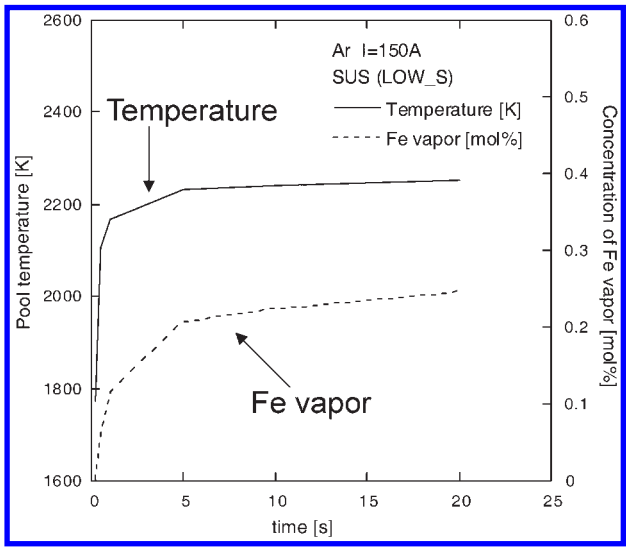

10 Relation between maximum weld pool temperature and maximum concentration of iron vapour in argon GTA welding

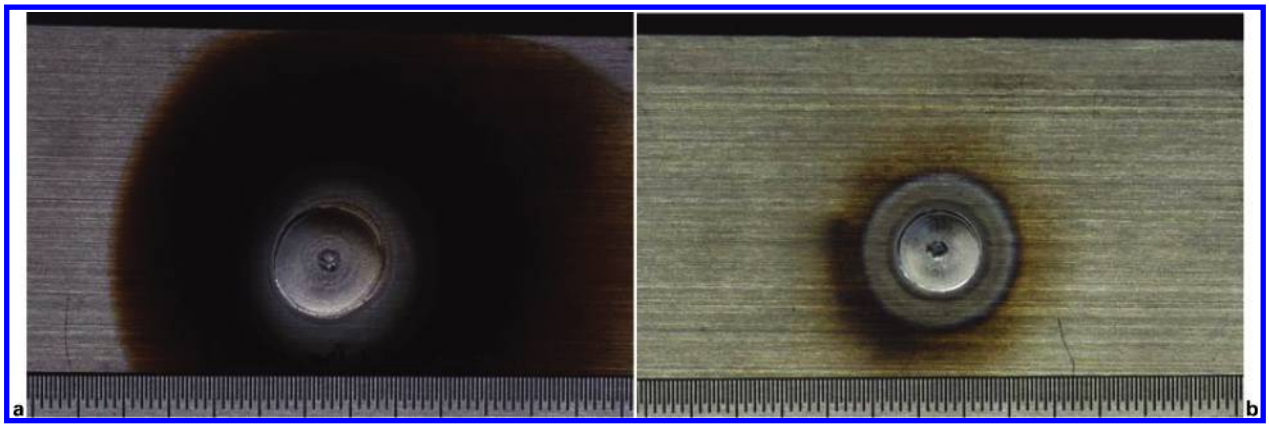

11 Surface appearances of SUS304 after stationary GTA welding for 20 s in *a* helium and in *b* argon

35 A mm^{-2}, while that decreases to 11 A mm^{-2} under the existence of iron vapour. Instead of the reduction of current density, electric conductivity is raised at the lower temperature region distant from the arc axis because of iron vapour as shown in Fig. 3 and thus, the arc current path considerably expands.

Figure 8 shows the calculation results of the two-dimensional distribution of temperature, weld penetration, fluid flow velocity and mole fraction of iron vapour at 20 s after arc ignition for argon gas shielding. The iron vapour concentration is significantly lower than that in the case of helium gas shielding shown in Fig. 5. The distribution of iron vapour is strongly influenced by plasma jet. The extent of its influence is higher than in the case of helium gas shielding because of the higher flow velocities near the anode in an argon arc.

Figure 9 and 10 show the calculation results of transient maximum concentration of iron vapour and transient maxmum temperature of the weld pool for helium gas and argon gas shielding respectively. It is seen that the iron vapour concentration increases with increasing weld pool temperature for both helium and argon shielding gas. However, the maximum temperature of the weld pool in argon shielding is lower by 500 K than that in helium shielding. As a result, the maximum concentration of iron vapour in argon shielding is $\sim$0·25 mol.-% that is one thirtieth of that in helium shielding. Because the total heat input and heat flux density are greater in helium shielding than in argon shielding, the surface temperature of the weld pool increased resulting in an increase in the amount of vapour in the arc.

The numerical calculation of weld arc simulation by the present model showed that the amount of metal vapour generated in GTA welding is higher in helium gas shielding than in argon shielding. This result coincides with the empirical fact that smut stuck on beads is significant in helium GTA. Figure 11 shows the appearance of the bead and its surroundings made by stationary GTA welding of SUS304 stainless steel plates for 20 s in helium gas shielding under the welding conditions in Fig. 5 and in argon gas shielding under those in Fig. 8 respectively. Smut observed as the black soot like deposit on the plate surrounding the weld bead is clearly higher in its amount in helium GTA than in argon GTA.

Conclusions

The authors developed a numerical model of the stationary GTA welding taking into account iron vapour from the weld pool surface and simulated the effect of iron vapour on the properties of the arc and weld pool. The main conclusions are summarised as follows.

1. In the stationary GTA welding of stainless steel in helium gas shielding, iron vapour is strongly influenced by high speed plasma flow and expands in the radial direction while its distribution is concentrated just above the weld pool surface beneath the arc.
2. The calculation and experiments about arc voltage satisfactorily coincide each other. The numerical simulation successfully reproduced the empirical fact that arc voltage in conventional GTA welding becomes lower than that in GTA welding on water cooled copper plates.
3. The welding current density distribution was calculated for the case of neglecting and not neglecting the mixture of iron vapour. It was found that mixture of iron vapour into arc plasma reduces the maximum current density and concurrently, the arc current path expands because of diffusion of iron vapour in the radial direction.
4. In argon gas shielding, the maximum concentration of iron vapour was found to decrease to one thirtieth of that in helium shielding because the maximum temperature of the weld pool is decreased by 500 K.

Acknowledgement

This work was supported by a grant-in-aid for Scientific Research (B) (2007) from the Japan Society for Promotion of Science (JSPS).

References

1. M. Tanaka, T. Watanabe, T. Isa and H. Nishiwaki: *J. Plasma Fusion Res.*, 2006, **82**, (8), 492–496.
2. H. G. Fan and R. Kovacevic: *J. Jpn Weld. Soc.*, 2007, **76**, (2), 82–89.
3. H. Nishiyama, T. Sawada, H. Takana, M. Tanaka and M. Ushio: *ISIJ Int.*, 2006, **46**, (5), 705–711.
4. M. Tanaka and J. J. Lowke: *J. Phys. D*, 2007, **40D**, 1–23.
5. S. Tashiro, M. Tanaka, K. Nakata, T. Iwao, F. Koshiishi, K. Suzuki and K. Yamazaki: *Sci. Technol. Weld. Joining*, 2007, **12**, (3), 202–207.
6. K. C. Hsu, K. Etemadi and E. Pfender: *J. Appl. Phys.*, 1983, **54**, 1293–1301.
7. M. Goodarzi, R. Choo and J. M. Toguri: *J. Phys. D*, 1997, **30D**, 2744–2756.
8. T. Zacharia, S. A. David, J. M. Vitek and T. DebRoy: *Metall. Trans. B*, 1990, **21B**, 600–603.

9. S. A. David, T. DebRoy and J. M. Vitek: *MRS Bull.*, 1994, **19**, 29–35.
10. T. Zacharia, S. A. David, J. M. Vitek and H. G. Kraus: *Weld. J.*, 1995, **74**, 353–362.
11. W. H. Kim, H. G. Fan and S. J. Na: *Numer. Heat Transfer A*, 1997, **32A**, 633–652.
12. H. G. Fan, H. L. Tsai and S. J. Na: *Int. J. Heat Mass Transfer*, 2001, **44**, 417–428.
13. C. Winkler, G. Amberg, H. Inoue, T. Koseki and M. Fujii: *Sci. Technol. Weld. Joining*, 2000, **5**, 8–20.
14. H. G. Fan and R. Kovacevic: *J. Phys. D*, 2004, **37D**, 2531–2544.
15. J. Menart and L. Lin: *Plasma Chem. Plasma Process.*, 1999, **19**, (2), 153–170.
16. R. L. O'Brien (ed.): 'Welding handbook', 8th edn, Vol. 2, 99; 1991, Miami, FL, American Welding Soceity.
17. H. Terasaki, M. Tanaka and M. Ushio: *Q. J. Jpn Weld. Soc.*, 2002, **20**, (2), 201–206.
18. C. R. Wilke: *J. Chem. Phys.*, 1950, **18**, (4), 517–519.
19. A. B. Murphy: *J. Phys. D*, 1996, **29D**, 1922–1932.
20. The Japan Institute of Metals: 'Data book of metals'; 3rd edn; 1993, Tokyo, Maruzen Co., Ltd.
21. A. B. Murphy: *Plasma Chem. Plasma Process.*, 1995, **15**, (2), 279–307.
22. S. Tashiro, M. Tanaka, M. Nakatani, M. Furubayashi and Y. Yamazaki: *Q. J. Jpn Weld. Soc.*, 2007, **25**, (1), 3–9.
23. M. Tanaka, H. Terasaki, M. Ushio and J. J. Lowke: *Metall. Mater. Trans. A*, 2002, **33A**, 2043–2052.